A radio structure resolved at the deca-parsec scale in the radio-quiet quasar PDS 456 with an extremely powerful X-ray outflow

Monthly Notices
of the
ROYAL ASTRONOMICAL SOCIETY

MNRAS **482,** 1701–1705 (2019) doi:10.1093/mnras/sty2798

A radio structure resolved at the deca-parsec scale in the radio-quiet quasar PDS 456 with an extremely powerful X-ray outflow

Jun Yang [1,2★] Tao An [2★] Fang Zheng,[2,3] Willem A. Baan [4,5] Zsolt Paragi,[6] Prashanth Mohan,[2] Zhongli Zhang[2] and Xiang Liu[4]

[1]*Department of Space, Earth and Environment, Chalmers University of Technology, Onsala Space Observatory, SE-439 92 Onsala, Sweden*
[2]*Shanghai Astronomical Observatory, Key Laboratory of Radio Astronomy, Chinese Academy of Sciences, 200030 Shanghai, China*
[3]*University of Chinese Academy of Sciences, 19A Yuquan Road, Shijingshan District, 100049 Beijing, China*
[4]*Xinjiang Astronomical Observatory, Key Laboratory of Radio Astronomy, Chinese Academy of Sciences, 150 Science 1-Street, 830011 Urumqi, China*
[5]*Netherlands Institute for Radio Astronomy ASTRON, NL-7991 PD Dwingeloo, the Netherlands*
[6]*Joint Institute for VLBI ERIC (JIVE), Postbus 2, NL-7990 AA Dwingeloo, the Netherlands*

Accepted 2018 October 9. Received 2018 September 17; in original form 2018 March 16

ABSTRACT

Active galactic nuclei (AGNs) accreting at rates close to the Eddington limit can host radiatively driven mildly relativistic outflows. Some of these X-ray absorbing but powerful outflows can produce strong shocks, resulting in a significant non-thermal emission. This outflow-driven radio emission might be detectable in the radio-quiet quasar PDS 456, as it has a bolometric luminosity that reaches the Eddington limit and a relativistic wide-aperture X-ray outflow with a kinetic power high enough to quench the star formation in its host galaxy. To investigate this possibility, we performed very-long-baseline interferometric (VLBI) observations of the quasar with the European VLBI Network (EVN) at 5 GHz. The full-resolution EVN image reveals two faint and diffuse radio components with a projected separation of about 20 pc and an average brightness temperature of around two million Kelvin. In relation to the optical submas-accuracy position measured by the *Gaia* mission, the two components are very likely on opposite sides of an undetected radio core. Thus, the VLBI structure at the deca-pc scale could be either a young jet or a bidirectional radio-emitting outflow, launched in the vicinity of a strongly accreting central engine. Two diffuse components at the hecto-pc scale, likely the relic radio emission from past AGN activity, are tentatively detected on each side in the low-resolution EVN image.

Key words: galaxies: active – quasars: individual: PDS 456 – radio continuum: galaxies.

1 INTRODUCTION

The accretion rate can regulate the radio emission in active galactic nuclei (AGNs) either directly in the form of wide-angle mildly relativistic winds (e.g. Yuan & Narayan 2014) or by supplementing the jet synchrotron emission. Statistical studies of AGNs indicate an anticorrelation between the accretion rate and the radio loudness (e.g. Greene, Ho & Ulvestad 2006; Panessa et al. 2007; Sikora, Stawarz & Lasota 2007). For accretion rates approaching the Eddington limit, AGNs tend to be radio-quiet (e.g. Greene et al. 2006). They can host powerful outflows, which can quench star-formation activity (e.g. Nardini et al. 2015; Tombesi et al. 2015; Tombesi 2016) and address the supermassive black hole–host galaxy coevolution through feedback (e.g. Kormendy & Ho 2013). Some high-speed (∼0.1 c) outflows might produce strong interactions or shocks and thus might create radio-emitting sources (e.g. Zakamska & Greene 2014; Nims, Quataert & Faucher-Giguère 2015). Very-long-baseline interferometric (VLBI) observations of optically luminous radio-quiet quasars will allow us to search for radio-emitting wide-angle but powerful outflows in order to provide direct evidence for this mode of AGN feedback (e.g. Giroletti et al. 2017; Wylezalek & Morganti 2018).

PDS 456 is a radio-quiet quasar at $z = 0.184$ (Simpson et al. 1999) with a black hole mass of $M_{\rm bh} \sim 10^9\,{\rm M}_\odot$ (Nardini et al. 2015). It is one of a few AGNs known to host an extremely powerful outflow ($\sim 10^{46}$ erg s^{-1}; Nardini et al. 2015; Tombesi 2016) and a compact radio counterpart (Yun et al. 2004). It is one of the most luminous quasars in the Universe at $z < 0.3$ (Simpson et al. 1999; Torres et al. 1997) and it has a bolometric luminosity of $L_{\rm bol} \sim 10^{47}$ erg s^{-1} (Reeves et al. 2000), close to its Eddington luminosity $L_{\rm Edd}$ (Nardini et al. 2015). X-ray spectroscopic observations indicate a powerful mildly relativistic outflow covering a solid angle of 3π and active over time-scales of years (Nardini et al. 2015; Matzeu

★ E-mail: jun.yang@chalmers.se (JY); antao@shao.ac.cn (TA)

et al. 2017). The X-ray outflow shows a tight correlation with the X-ray luminosity, indicating that the outflow is likely driven by the radiation pressure (Matzeu et al. 2017). The radio counterpart of PDS 456 has an optically thin spectrum with relatively high flux densities (i.e. 24 ± 5 mJy at 1.2 GHz and 4.5 ± 0.9 mJy at 8.4 GHz) and a spectral index of −0.85 ± 0.10, and it shows a point-source structure in the Very Large Array (VLA) images (Yun et al. 2004). As the radio continuum luminosity is nearly an order of magnitude higher than the estimated far-infrared luminosity, AGN activity was inferred to dominate the source radio emission (Yun et al. 2004). To investigate the origin of the radio emission and association with AGN activity, we performed very high-resolution imaging observations of PDS 456 with the European VLBI Network (EVN) at 5 GHz.

This paper is organized as follows. In Section 2, we describe the EVN experiment and the data reduction. In Section 3, we present the source radio morphology on subkpc scales. In Section 4, we discuss the radio core, the AGN activity and the origin of the radio VLBI structure. We give concluding remarks in Section 5. Throughout the paper, a standard ΛCDM cosmological model with $H_0 = 71\,\mathrm{km\,s^{-1}\,Mpc^{-1}}$, $\Omega_\mathrm{m} = 0.27$ and $\Omega_\Lambda = 0.73$ is adopted; the images then have a scale of 3.1 pc mas^{-1}.

2 OBSERVATIONS AND DATA REDUCTION

We observed PDS 456 with the e-EVN at 5 GHz on 2016 February 3. During the observations, each station had a data transferring speed of 1024 Mbps (16 sub-bands in dual polarization, 16 MHz per sub-band, 2-bit quantization). The correlation was performed in real-time mode by the EVN software correlator (SFXC; Keimpema et al. 2015) at the Joint Institute for VLBI, ERIC (JIVE) using a 2-s integration time and 32 frequency points per sub-band. The participating EVN stations included Effelsberg, Medicina, Noto, Onsala, Torun, Yebes, Westerbork (single antenna) and Hartebeesthoek.

The e-EVN observations of PDS 456 were performed with the phase-referencing technique. The compact source J1724−1443 (about 59 arcmin distant) was employed as the phase-referencing calibrator. Its position is RA $= 17^\mathrm{h}24^\mathrm{m}46\overset{\mathrm{s}}{.}96656$, Dec. $= -14^\circ43'59\overset{''}{.}7610$ (J2000) in the source catalogue from the Goddard Space Flight Centre VLBI group. In the existing geodetic VLBI observations, the calibrator had a correlation amplitude of $\gtrsim$0.15 Jy at 8.4 GHz on the long baselines. The correlation position for PDS 456 is RA $= 17^\mathrm{h}28^\mathrm{m}19\overset{\mathrm{s}}{.}7920$, Dec. $= -14^\circ15'55\overset{''}{.}912$ (J2000). The nodding observations used a cycle period of about 4 min (1.5 min for J1724−1443 and 2.5 min for PDS 456) and lasted a total of about 2 h. All telescopes had an elevation of ≥17 deg during the observations. Besides the pair of sources, a bright flat-spectrum radio quasar NRAO 530 (e.g. An et al. 2013) was also observed to enable the determination of instrumental bandpass shapes.

The data were calibrated using the National Radio Astronomy Observatory (NRAO) software package Astronomical Image Processing System (AIPS; Greisen 2003). A priori amplitude calibration was performed with the system temperatures and the antenna gain curves. The ionospheric dispersive delays were corrected according to a map of total electron content provided by Global Positioning System (GPS) satellite observations. Phase errors due to antenna parallactic angle variations were removed. A manual phase calibration was carried out with a 2-min scan of NRAO 530 data. After the instrumental phase delays were removed, the global fringe-fitting and the bandpass calibration were performed.

We first imaged the phase-referencing source J1724−1443 using a loop of model fitting and self-calibration in DIFMAP (Shepherd, Pearson & Taylor 1994). Then, we re-ran fringe-fitting to remove its structure-dependent phase errors in AIPS in the second iteration. The calibrator J1724−1443 has a single-side core–jet structure with a total flux density of 0.37 ± 0.02 Jy. Its radio core (i.e. the jet base) is a point source with a flux density of 0.16 ± 0.01 Jy and its position was used as the reference point in the phase-referencing calibration. We also ran amplitude and phase self-calibrations on the data of J1724−1443 and transferred the solutions to the data of PDS 456.

Because of the limited *uv* coverage in particular on the long baselines, the deconvolution was performed by fitting the visibility data of PDS 456 directly to some circular Gaussian models in DIFMAP to minimize the potential deconvolution errors of CLEAN. The model-fitting results are reported in Table 1.

3 VLBI IMAGING RESULTS OF PDS 456

The CLEAN maps of PDS 456 are shown in Fig. 1. There are two faint radio components detected with a projected distance of 19 pc and a relative position angle of 146°, marked as C1 and C2 in the left panel. Two more components, X1 and X2, are tentatively detected at much larger scales, as shown in the right panel.

The two-component structure in component C is present even when studying dirty maps (i.e. without running de-convolution). Compared to the dirty beam, the noise pattern convolved with component C is much smoother and wider along the extension direction in the initial dirty map with natural weighting. Component C is clearly seen with a peak brightness: 0.64 mJy beam^{-1} (signal-to-noise ratio ∼16) when all the baselines within Europe (≤33 Mλ, where λ is the wavelength) are included. However, it is not observed up to an upper limit of 0.3 mJy beam^{-1} (3σ) using the long baselines of ≥103 Mλ between the European stations and Hartebeesthoek. Because of this significant decrease in peak brightness, a single point-source structure can be firmly excluded.

Assuming no significant variability, the flux density of component C represents only 16 per cent of that measured with the VLA (8.2 mJy at 5 GHz; Reeves et al. 2000). Employing a strong Gaussian tapering (e.g. 0.5 at 5 Mλ), two additional diffuse components X1 and X2 at a projected separation of about 550 pc are marginally detected. As the detections are mainly dependent on the shortest baseline (Effelsberg–Westerbork), it is hard to properly image and locate these faint extended structures. With the inclusion of these two components, about 68 per cent of the VLA flux density is still unaccounted for in our VLBI image. As a portion of this missing emission is likely to be associated with these VLBI components, both the total flux density and the size reported in Table 1 are considered to be lower limits.

All the components have relatively low average brightness temperatures, $T_\mathrm{b} \lesssim 10^6$ K. In Table 1, T_b is estimated as (e.g. Condon et al. 1982)

$$T_\mathrm{b} = 1.22 \times 10^9 \frac{S_\mathrm{int}}{\nu_\mathrm{obs}^2 \theta_\mathrm{size}^2}(1+z), \quad (1)$$

where S_int is the integrated flux density (in mJy), ν_obs is the observation frequency (in GHz), θ_size is the FWHM of the circular Gaussian model (in mas) and z is the redshift.

Table 1. Circular Gaussian model-fitting results of the radio components detected in PDS 456 with the e-EVN observations at 5 GHz. Columns give (1) component name, (2) right ascension, (3) declination, (4) positional error (including an error of 0.24 mas from the reference source), (5) peak brightness, (6) integrated flux density, (7) FWHM, (8) average brightness temperature, (9) fraction with respect to the VLA total flux density measurement at 5 GHz (Reeves et al. 2000) and (10) radio luminosity.

Component	R.A. (J2000)	Dec. (J2000)	σ_p (mas)	S_{peak} (mJy beam^{-1})	S_{int} (mJy)	θ_{size} (mas)	T_b (10^6 K)	S_{evn}/S_{vla}	L_r (10^{39} erg s^{-1})
C1	$17^h28^m19\overset{s}{.}78967$	$-14°15'55\overset{''}{.}8550$	0.4	0.36 ± 0.03	1.09	6.9	1.4	0.13	5.5
C2	$17^h28^m19\overset{s}{.}78943$	$-14°15'55\overset{''}{.}8499$	0.6	0.18 ± 0.03	0.29	2.6	2.6	0.04	1.7
X1	$17^h28^m19\overset{s}{.}79224$	$-14°15'55\overset{''}{.}9544$	1.9	0.47 ± 0.07	0.78	15.7	0.2	0.09	3.8
X2	$17^h28^m19\overset{s}{.}78523$	$-14°15'55\overset{''}{.}8030$	2.2	0.40 ± 0.07	0.48	6.5	0.7	0.06	2.5

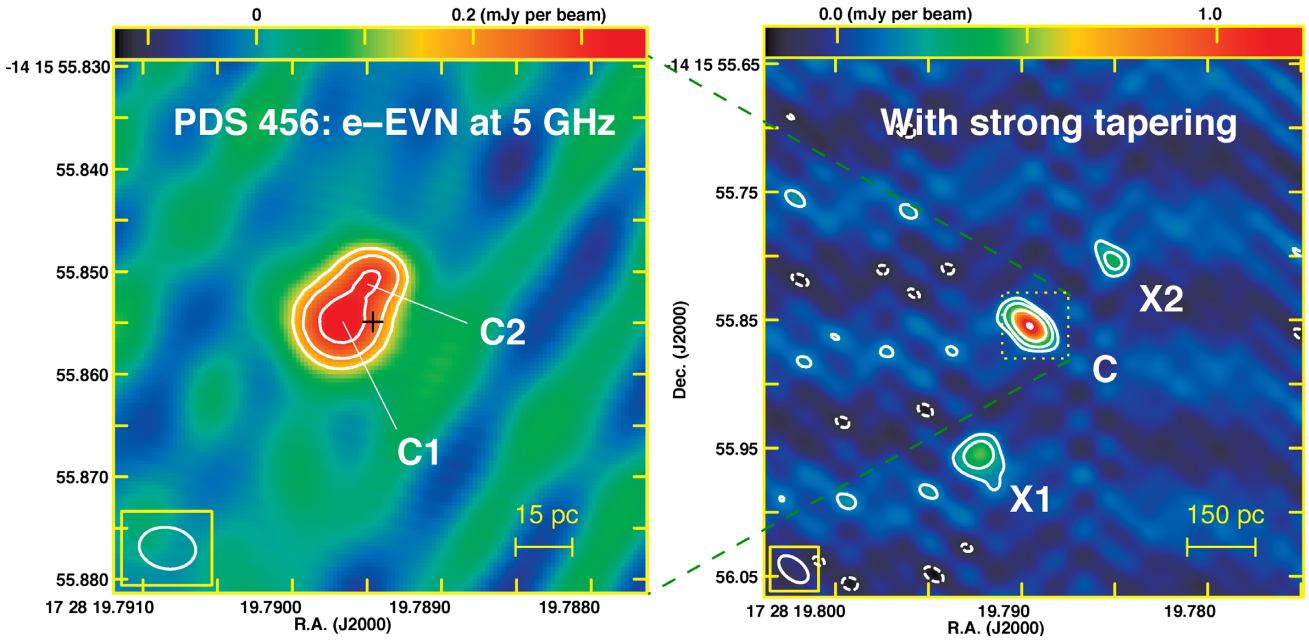

Figure 1. The CLEAN images of the optically luminous radio-quiet quasar PDS 456 observed with the e-EVN at 5 GHz. Left: firm detections of two faint and diffuse components C1 and C2 with natural weighting and slightly Gaussian tapering (0.2 at the *uv* radius 120 Mλ). The black cross marks the submas-accuracy optical centroid measured by *Gaia*. The full width at half-maximum (FWHM) of the synthesized beam is 5.5×4.4 mas^2 at 81.2 deg. The contours are $0.09 \times (-1, 1, 1.4, 2)$ mJy beam^{-1}. The image peak is 0.36 mJy beam^{-1}. Right: tentative detections of two more diffuse radio components X1 and X2 on subkpc scales with natural weighting and strong Gaussian tapering (0.5 at the *uv* radius 5 Mλ). The beam FWHM is 27.1×15.5 mas^2 at 50.1 deg. The contours are $0.15 \times (-1, 1, 2, 4, 8)$ mJy beam^{-1}. The image peak is 1.23 mJy beam^{-1}. All the characteristic parameters related to these components are summarized in Table 1. The first contours in both images are at the 3σ level.

4 DISCUSSION

4.1 Radio AGN activity

All VLBI-detected components are located within the optical nuclear region of PDS 456. The centroid of its optical emission (J2000, RA = $17^h28^m19\overset{s}{.}789380$, Dec. = $-14°15'55\overset{''}{.}85543$, σ_p = 0.04 mas), published by the second data release (DR2; Brown et al. 2018) of the *Gaia* mission (Prusti et al. 2016), is marked as a black cross in the left panel of Fig. 1. As the residuals from the point-source model fitting statistically agree with the assumed observational noise, the astrometric excess noise for PDS 456 is insignificant (i.e. 0 mas) in the *Gaia* DR2 catalogue. The extremely compact optical morphology then allows us to take the optical centroid as a robust marker of the central supermassive black hole hosted in the optical nucleus. The components C1 and C2 have offsets of 4.2 ± 0.4 mas and 5.5 ± 0.6 mas, respectively, with respect to the optical centroid.

As the resolved components C1 and C2 have significant offsets from the optical centroid, they might not be associated with the radio core, i.e. the base of a well-collimated (mildly) relativistic jet with a flat spectrum. If components C1 and C2 are a pair of episodic ejecta or a radio-emitting wind-like outflow, driven by the central engine, the radio core would be expected at a position near the centre of the pair of components. Assuming that the radio core has a point-source structure, we can set a 3σ upper limit of 0.3 mJy on the total flux density of the hidden radio core with the data on the long baselines to Hartebeesthoe only. This gives a radio luminosity of $L_r = \nu L_\nu \leq 1.3 \times 10^{39}$ erg s^{-1}.

While there is no evidence for a compact and partially self-absorbed radio core, there seems to be ample evidence for AGN activity as a dominant source of the faint radio structure on subkpc scales in PDS 456. All the VLBI components in Fig. 1 are located roughly along a line in the north-west–south-east direction. This structural alignment can be formed naturally by AGN activity. It is difficult to associate these radio components with supernovae remnants produced by star-formation activity. A supernova can have a peak monochromatic luminosity up to $L_\nu \sim 10^{29}$ erg s^{-1} Hz^{-1} at 5 GHz (Weiler et al. 2002). While these VLBI components have

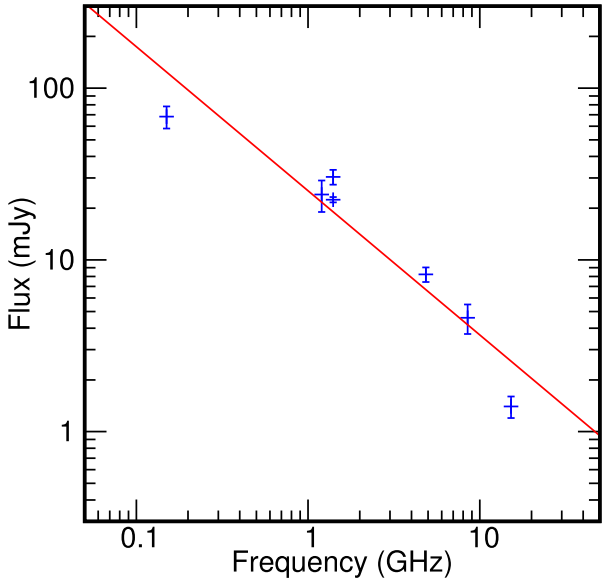

Figure 2. The radio spectrum of PDS 456 observed from 150 MHz to 15 GHz. The red line represents the simple model of $S_\nu = S_0\nu^\alpha$, where $S_0 = 25 \pm 4$ mJy and $\alpha = -0.84 \pm 0.11$.

monochromatic luminosities $L_\nu \geq 2.7 \times 10^{29}$ erg s^{-1} Hz^{-1} at 5 GHz and extended structures, it is certainly hard to attribute any component to a single young supernova. Additionally, because PDS 456 is not a starburst galaxy like Arp 220 (Yun et al. 2004), we do not expect to observe a great number of supernova remnants in the nuclear region.

The radio AGN activity in PDS 456 is relatively recent. The outer components X1 and X2 represent the largest structure at a projected separation of about 0.55 kpc and likely constitute bright relic radio emission from past AGN activity. Assuming a constant apparent expansion speed of 0.2 c (e.g. Owsianik & Conway 1998) for young radio sources (typically $\lesssim 10^6$ yr; e.g. Fanti et al. 1995), they have an age of 10^4 yr. According to the correlation relation between the linear size and the turnover frequency observed in young and bright radio sources (O'Dea 1998), the observed linear size allows us to predict a turnover at a frequency of about 1 GHz for PDS 456. Fig. 2 displays the radio spectrum of PDS 456 between 0.15 and 15 GHz. Besides the flux densities reported by Yun et al. (2004), we have added two more measurements. The Giant Metrewave Radio Telescope (GMRT) observations gave a total flux density of 68 ± 10 mJy at 150 MHz (Intema et al. 2017). According to the existing VLA archive data (project: AL501) calibrated by the VLA pipeline, a 15-GHz flux density of 1.4 ± 0.1 mJy was measured. The red line in Fig. 2 is a power-law fit to the data with a best-fitting spectral index of -0.84 ± 0.11. The source does not show a distinct turnover at frequencies $\geq$0.15 GHz. The relatively steep spectral index and an integrated flux density, dominated by diffuse structures undetected by VLBI, indicate a paused or slow expansion from early on; these are then in a dying or decaying state.

4.2 Component C: outflow-driven versus jet-driven

Components C1 and C2 might originate from a bidirectional radio-emitting outflow, in view of their diffuse and faint radio structure. A high-speed, wide-opening-angle and persistent outflow has been indirectly observed in multiple X-ray spectral observations (e.g. Matzeu et al. 2017; Nardini et al. 2015; Reeves et al. 2018) with reports of multiple velocity components, up to 0.46 c (Reeves et al. 2018). An ultraviolet outflow at 0.3 c has also been recently reported by Hamann et al. (2018). From a sample of 568 luminous quasars, Zakamska & Greene (2014) find a strong association between powerful outflows and the radio luminosity in radio-quiet AGNs; this is indicative of the radio emission originating from shocks driven by the outflow with a conversion efficiency of $\sim 10^{-4}$ between the radio luminosity and the outflow kinetic power. Component C has a radio luminosity of $L_r = 7 \times 10^{39}$ erg s^{-1}, a factor of 3×10^{-7} lower than the kinetic power of the X-ray outflow (2×10^{46} erg s^{-1}; Nardini et al. 2015). If the radio emission is indeed wind-like and outflow-driven, the conversion efficiency is significantly lower than the typical value of 10^{-4}. The X-ray outflow then has sufficient kinetic power to drive shocks that produce the observed radio emission.

The VLBI morphology resembles compact symmetric objects (CSOs) characterized by two-sided mini-lobes or hotspots at the subkpc scales (e.g. Wilkinson et al. 1994; Readhead et al. 1996; Xiang et al. 2005). PDS 456 can then be identified as a candidate CSO. Because of the interaction between jets and the surrounding interstellar medium, CSOs usually have mildly relativistic speeds (e.g. Owsianik & Conway 1998; Polatidis & Conway 2003; An et al. 2012). Assuming an intrinsically symmetric ejection and a spectral index of 0.85 (i.e. the same as the VLA total flux density measurement), the observed flux ratio between components C1 and C2 implies that $\beta \cos\theta_v = 0.17\,c$, where β is the intrinsic jet speed and θ_v is the viewing angle (e.g. Böttcher, Harris & Krawczynski 2012). If the jet is directed close to the line of sight (e.g. $\theta_v \lesssim 8^\circ$; Yun et al. 2004), this still gives an intrinsically low jet speed ($\beta \sim \beta\cos\theta_v$). Sokolovsky et al. (2011) reported $T_b \gtrsim 10^8$ K for a sample of 64 candidate CSOs with much higher radio power. Compared with the sample, the two components have a brightness temperature two orders of magnitude lower and a significantly expanded structure, thus indicating that they likely constitute a pair of young but dying ejecta. Amongst samples of symmetric radio sources with known radio luminosities (e.g. Kunert-Bajraszewska et al. 2010; An & Baan 2012; Kunert-Bajraszewska 2016), they have a relatively low radio power and might fail to significantly expand in size.

Compared with a scenario involving collimated jets, the expectation of outflow-driven radio emission should enable the observation of a biconical radio structure near the supermassive black hole with a much wider opening angle (e.g. $\sim$100°) based on modelling the P Cygni profile in the broad-band X-ray spectrum of PDS 456 (Nardini et al. 2015). Our high-resolution VLBI image tentatively supports this wide-opening-angle outflow scenario. Assuming that the radio emission at the deca-pc scale comes from strong shocks of the outflow and that the outflow driver is centrally located between C1 and C2, a rough estimate of the opening angle is $\sim$130° based on component C1 and $\sim$50° from component C2. The intrinsic opening angle might be much smaller than the observed opening angle because of the projection effect. To obtain a reliable estimate of the opening angle, it is necessary to use additional epochs of VLBI observations, because our size estimates are inaccurate in the direction vertical to the outflow axis as a result of the limited *uv* coverage and the use of a circular Gaussian model.

Regardless of which scenario is likely in PDS 456, our results clearly establish the association between radio emission and AGN activity. Because of the diffuse two-sided faint structure, there is no strong Doppler beaming effect. In the scenario of the outflow-driven radio emission, PDS 456 would be the most promising source for a future observational confirmation amongst radio-quiet quasars. To date, clearly positive cases for the scenario have not been identified

(e.g. Wylezalek & Morganti 2018). In the only previously known candidate, IRAS 17020+4544, the non-thermal radio emission and the ultra-fast X-ray outflow are both powered by the central engine (Giroletti et al. 2017). In comparison, here the powerful X-ray outflow is expected to be the driver of the nuclear radio emission. In the alternative scenario (i.e. jet-driven emission), PDF 456 would then be a rare example of intermittent and low-power jet activity amongst sources accreting at rates close to the Eddington limit (e.g. Greene et al. 2006).

5 CONCLUSIONS

In order to understand the origin of compact radio emission from the nuclear region, we have observed the optically and X-ray luminous but radio-quiet quasar PDS 456 with the e-EVN at 5 GHz. In the full-resolution image, we found two faint and diffuse radio components with a separation of about 20 pc and an average brightness temperature of around two million Kelvin. In relation to the submas-accuracy *Gaia* position, the two components are putatively located on opposite sides of an unobserved radio core. The radio structure indicates recent jet-driven AGN activity at a low radio power. The new VLBI observations also indicate that the radio emission likely originates from the shocks produced by the X-ray outflows when interacting with the surrounding external medium. Additional subkpc-scale diffuse components are tentatively detected in the low-resolution image and appear to be relic radio emission from earlier AGN activity. Future VLBI imaging observations can be employed to provide more conclusive evidence to support the outflow-driven scenario and, hence, to clarify the origin of radio emission in this source.

ACKNOWLEDGEMENTS

This work was partly supported by the SKA pre-research funding from the Ministry of Science and Technology of China (2018YFA0404600) and the Chinese Academy of Sciences (CAS, No. 114231KYSB20170003). TA is grateful for the grant provided by the Youth Innovation Promotion Association of CAS. The European VLBI Network is a joint facility of independent European, African, Asian and North American radio astronomy institutes. Scientific results from data presented in this publication are derived from the following EVN project code(s): EY024A. The National Radio Astronomy Observatory is a facility of the National Science Foundation operated under cooperative agreement by Associated Universities, Inc. This work has made use of data from the European Space Agency (ESA) mission *Gaia* (https://www.cosmos.esa.int/gaia), processed by the *Gaia* Data Processing and Analysis Consortium (DPAC, https://www.cosmos.esa.int/web/gaia/dpac/consortium). Funding for the DPAC has been provided by national institutions, in particular the institutions participating in the *Gaia* Multilateral Agreement. We thank the staff of the GMRT who made these observations possible. The GMRT is run by the National Centre for Radio Astrophysics of the Tata Institute of Fundamental Research.

REFERENCES

An T., Baan W. A., 2012, ApJ, 760, 77
An T. et al., 2012, ApJS, 198, 5
An T., Baan W. A., Wang J-Y., Wang Y., Hong X-Y., 2013, MNRAS, 434, 3487
Böttcher M., Harris D. E., Krawczynski H., 2012, Relativistic Jets from Active Galactic Nuclei. Wiley, Weinheim
Brown A. G. A.Gaia Collaboration et al.(Gaia Collaboration), 2018, A&A, 616, A1
Condon J. J., Condon M. A., Gisler G., Puschell J. J., 1982, ApJ, 252, 102
Fanti C., Fanti R., Dallacasa D., Schilizzi R. T., Spencer R. E., Stanghellini C., 1995, A&A, 302, 317
Giroletti M., Panessa F., Longinotti A. L., Krongold Y., Guainazzi M., Costantini E., Santos-Lleo M., 2017, A&A, 600, A87
Greene J. E., Ho L. C., Ulvestad J. S., 2006, ApJ, 636, 56
Greisen E. W., 2003, in Heck A., ed., Astrophysics and Space Science Library, Vol. 285, Information Handling in Astronomy: Historical Vistas. Kluwer, Dordrecht, p. 109
Hamann F., George C., Reeves J., Nardini E., 2018, MNRAS, 476, 943
Intema H. T., Jagannathan, P., Mooley K. P., Frail D. A., 2017, A&A, 598, A78
Keimpema A. et al., 2015, Exp. Astron., 39, 259
Kormendy J., Ho L. C., 2013, ARA&A, 51, 511
Kunert-Bajraszewska M., 2016, Astron. Nachr., 337, 27
Kunert-Bajraszewska M., Gawroński M. P., Labiano A., Siemiginowska A., 2010, MNRAS, 408, 2261
Matzeu G. A., Reeves J. N., Braito V., Nardini E., McLaughlin D. E., Lobban A. P., Tombesi F., Costa M. T., 2017, MNRAS, 472, L15
Nardini E. et al., 2015, Science, 347, 860
Nims J., Quataert E., Faucher-Giguère C.-A., 2015, MNRAS, 447, 3612
O'Dea C. P., 1998, PASP, 110, 493
Owsianik I., Conway J. E., 1998, A&A, 337, 69
Panessa F., Barcons X., Bassani L., Cappi M., Carrera F. J., Ho L. C., Pellegrini S., 2007, A&A, 467, 519
Polatidis A. G., Conway J. E., 2004, PASA, 20, 69
Prusti T., et al., 2016, A&A, 595, A1
Readhead A. C. S., Taylor G. B., Xu W., Pearson T. J., Wilkinson P. N., Polatidis A. G., 1996, ApJ, 460, 612
Reeves J. N., O'Brien P. T., Vaughan S., Law-Green D., Ward M., Simpson C., Pounds K. A., Edelson R., 2000, MNRAS, 312, L17
Reeves J. N., Braito V., Nardini E., Lobban A. P., Matzeu G. A., Costa M. T., 2018, ApJ, 854, L8
Shepherd M. C., Pearson T. J., Taylor G. B., 1994, BAAS, 26, 987
Sikora M., Stawarz Ł., Lasota J.-P., 2007, ApJ, 658, 815
Simpson C., Ward M., O'Brien P., Reeves J., 1999, MNRAS, 303, L23
Sokolvsky K. V., Kovalev Y. Y., Pushkarev A. B., Mimica P., Perucho M., 2011, A&A, 535, A24
Tombesi F., 2016, Astron. Nachr., 337, 410
Tombesi F., Meléndez M., Veilleux S., Reeves J. N., González-Alfonso E., Reynolds C. S., 2015, Nature, 519, 436
Torres C. A. O., Quast G. R., Coziol R., Jablonski F., de la Reza R., Lépine J. R. D., Gregório-Hetem J., 1997, ApJ, 488, L19
Weiler K. W., Panagia N., Montes M. J., Sramek R. A., 2002, ARA&A, 40, 387
Wilkinson P. N., Polatidis A. G., Readhead A. C. S., Xu W., Pearson T. J., 1994, MNRAS, 269, 67
Wylezalek D., Morganti R., 2018, Nature Astronomy, 2, 181
Xiang L., Dallacasa D., Cassaro P., Jiang D., Reynolds C., 2005, A&A, 434, 123
Yuan F., Narayan R., 2014, ARA&A, 52, 529
Yun M. S., Reddy N. A., Scoville N. Z., Frayer D. T., Robson E. I., Tilanus R. P. J., 2004, ApJ, 601, 723
Zakamska N. L., Greene J. E., 2014, MNRAS, 442, 784

This paper has been typeset from a TEX/LATEX file prepared by the author.